Vaporization and thermodynamics of forsterite-rich olivine and some implications for silicate atmospheres of hot rocky exoplanets

Gustavo C.C. Costa [a, *], Nathan S. Jacobson [a], Bruce Fegley Jr. [b]

[a] NASA Glenn Research Center, 210 0 0 Brookpark Road, MS 106-1, Cleveland, OH, 44135, USA [b] Planetary Chemistry Laboratory, McDonnell Center for the Space Sciences, Department of Earth and Planetary Sciences, Washington University in St. Louis, Campus Box 1169, 1 Brookings Dr, St. Louis, MO, 63130-4899, USA

articleinfo

Article history:
Received 12 May 2016
Revised 16 November 2016 Accepted 14 February 2017
Available online 16 February 2017

abstract

We describe an experimental and theoretical study of olivine [Mg_2SiO_4 (Fo)–Fe_2SiO_4 (Fa)] vaporization The vaporization behavior and thermodynamic properties of a fosterite-rich olivine ($Fo_{95}Fa_5$) have been explored by high-temperature Knudsen effusion mass spectrometry (KEMS) from 1750 to 2250 K. The gases observed (in order of decreasing partial pressure) are Fe, SiO, Mg, O_2 and O. We measured the solidus temperature (~2050 K), partial pressures of individual gases, the total vapor pressure, and thermodynamic activities and partial molar enthalpies of MgO, 'FeO', and SiO_2 for the $Fo_{95}Fa_5$ olivine. The results are compared to other measurements and models of the olivine system. Our experimental data show olivine vaporizes incongruently. We discuss this system both as a psuedo-binary of Fo-Fa and a psuedo-ternary of MgO–'FeO'–SiO_2. Iron/magnesium molar ratios in the sample before (~0.05) and after (~0.04) vaporization are consistent with the small positive deviations from ideality of fayalite ($\gamma \sim 1.17$) in olivine of the composition studied (e.g., Nafziger and Muan, 1967). Our data for olivine + melt confirm prior theoretical models predicting fractional vaporization of Fe relative to Mg from molten silicates (Fegley and Cameron, 1987 ; Schaefer and Fegley, 2009; Ito et al., 2015). If loss of silicate atmospheres occurs from hot rocky exoplanets with magma oceans the residual planet may be enriched in magnesium relative to iron.

1. Introduction

We studied vaporization of olivine $(Mg_xFe_{1-x})_2SiO_4$ because it is one of the major silicate minerals that make up rocky planets in our solar system and presumably in extrasolar planetary systems (see below). The major gases produced by olivine vaporization (Fe, Mg, SiO, O_2, and O) are calculated to be abundant over wide P, T ranges in the atmospheres of hot, rocky extrasolar planets such as CoRoT-7b (e.g., Schaefer and Fegley, 2009 ; Ito et al., 2015). One purpose of our work is to provide reliable experimental vapor pressure data for olivine that can be used to test published calculations and guide future experimental work and spectroscopic observations.

Olivine contains the three most abundant elements (Mg, Si, Fe) in solar composition material that combine with oxygen to form rock (Lodders, 2003). The atomic abundances of Mg, Si, and Fe are similar to one another (within 20%) and are 1.03×10^6 (Mg), 1.00×10^6 (Si), and 0.848×10^6 (Fe) on the cosmochemical scale.

* Corresponding author.
E-mail address: gustavo.costa@nasa.gov (G.C.C. Costa).

http://dx.doi.org/10.1016/j.icarus.2017.02.006 0019-1035/

All other elements that combine with oxygen to form rock are sig- nificantly less abundant, e.g., Al (0.0846×10^6), Ca (0.0604×10^6), Na (0.0577×10^6), Ni (0.049×10^6), Mn (0.00922×10^6), K ($0.0\,0376 \times 10^6$), and Ti ($0.0\,0247 \times 10^6$). Spectroscopic studies of main sequence F and G stars with near-solar metallicity show constant ratios of Fe, Mg, and Si to one another (Section 3.4.7 in Lodders et al., 2009). Consequently olivine (and its high pressure polymorphs) is probably the major mineral in rocky exoplanets.

Magnesian (forsterite–rich) olivine with an average composi- tion of $(Mg_{0.9}Fe_{0.1})_2SiO_4$ is the dominant mineral in peridotite; the rock comprising Earth's upper mantle (Palme and O'Neill, 2014). Olivine is a solid solution between the end members forsterite (Fo:

Mg_2SiO_4) and fayalite (Fa: Fe_2SiO_4) with continuous variation of the solidus and liquidus curves from the melting point of the lower melting component (Fayalite 1490 K, $_{fus}H°= 89.3 \pm 1.1$ kJ mol^{-1}) to the melting point of the higher melting component (Forsterite 2163 K, $_{fus}H°= 102.8 \pm 5$ kJ mol^{-1}); in other words a cigar–shaped phase diagram (Bowen and Schairer, 1935, see Fig. 9). Melting be- gins at the solidus temperature and is completed at the liquidus temperature. Throughout this paper we use the terms "melting point" and "solidus" interchangeably.

Forsterite-rich olivine is present in the Earth's crust as an im- portant constituent of mafic and ultramafic igneous rocks and also is found in thermally metamorphosed, dolomitic limestones (Liebau, 2012). Moreover, it has important technological applica- tions in the ceramic and metallurgic industries, and in catalysis given its chemical and structural properties (Swierczynski et al., 2006). Olivine is also present in extra-terrestrial bodies such as the Moon, Mars, asteroids, meteorites, comets, interplanetary dust particles and circumstellar dust shells (Keil et al., 1970; Hoefen et al., 2003; Cruikshank and Hartmann, 1984; Nguyen and Zinner, 2004; Campins and Ryan, 1989; Bradley et al., 1992; Woolf and Ney, 1969).

Olivine is an orthosilicate mineral and naturally occurring forsterite-rich olivine adopts an orthorhombic (space group *Pbnm*) symmetry (Liebau, 2012). In this structure [SiO_4] tetrahedra are isolated and cross-linked by chains of edge-sharing, distorted oc- tahedra [MO_6] occupied by divalent cations (M) such as Mg^{2+} and Fe^{2+} (Liebau, 2012). Minor amounts of other divalent cations (e.g. Ca^{2+}, Mn^{2+} and Ni^{2+}) can also occupy the octahedra [MO_6] crystallographic sites and are commonly found in natural olivines (Liebau, 2012). As noted above Ca, Mn, and Ni are significantly less abundant than Mg or Fe and to good first approximation naturally occurring olivine is a binary solid solution between forsterite and fayalite. The Mg and Fe content in the solid solution of olivine and minor amounts of other divalent cations in its structure, which are common in natural olivine, are expected to affect vaporization and its thermodynamic properties by introducing activation energy for vaporization, leading to rate control by diffusion through different bonding strength and atomic structural configuration, affecting sur- face energy, the free energy of desorption, and the activation free energy for surface diffusion (Hirth, 1967; Navrotsky, 1978). Thus, it is important that the sample is fully structurally and chemically characterized before and after vaporization experiments (see be- low) in order to understand at the microscopic atomic level possi- ble discrepancies between different experiments, and experimental and theoretical thermodynamic results.

Given the importance of the MgO–'FeO'–SiO_2 system, there are a very large number of experimental and theoretical studies of its thermodynamics and phase relationships. Strictly speaking (as noted by Bowen and Schairer, 1935) the MgO–'FeO'–SiO_2 system is pseudo-ternary (and the FeO–SiO_2 subsystem is pseudo-binary) because there is always a small amount of ferric iron present in the liquid in equilibrium with FeO-bearing pyroxenes and olivine, which melt incongruently with separation of iron metal and silica. For example, Bowen and Schairer (1932) showed this for melting of pure fayalite and Stebbins and Carmichael (1984) confirmed their results; the melting reaction is

$$Fe_2SiO_4(\text{fayalite}) = 0.9620Fe_2SiO_4(\text{liq}) + 0.0253Fe_2O_3(\text{liq}) + 0.0380SiO_2(\text{liq}) + 0.0253Fe(\text{metal}) \quad (1)$$

The molar ratio of Fe^{3+}/Fe^{2+} is ~0.026 in the melt. However the Mg_2SiO_4–Fe_2SiO_4 system has always been treated as a binary system because ferric iron, although present, is only a minor com- ponent. We will return to this point later in the discussion.

The forsterite–fayalite solid solution has small positive devia- tions from ideality. There is no statistically significant excess en- tropy of mixing (Dachs and Geiger, 2007), so a symmetric reg- ular solution model with one parameter, as recommended by many groups (e.g., Dachs and Geiger, 2007; von Seckendorff and O'Neill, 1993; Wiser and Wood, 1991; Kitayama and Katsura, 1968; Larimer, 1968; Nafziger and Muan, 1967) is sufficient for describ- ing the small amounts of non-ideality. The Mg^{2+} and Fe^{2+} cations are distributed on the M1 and M2 octahedral sites in olivine (Muan, 1967; Nafziger and Muan, 1967) so equations for activity coefficients and exchange equilibria of forsterite and fayalite are written in terms of one half formula unit, e.g. $MgSi_{0.5}O_2$ (= ½ Mg_2SiO_4) and $FeSi_{0.5}O_2$ (= ½ Fe_2SiO_4). The activities of $MgSi_{0.5}O_2$ and $FeSi_{0.5}O_2$ have been determined by several different meth- ods including Fe-Mg partitioning between olivine and orthopyrox- ene and Fe-Mg partitioning between olivine and coexisting mag- nesiowüstites. In their classic paper on this system, Nafziger and Muan (1967) determine activities and phase boundaries by several equilibration methods. There are several measurements of a(FeO) and in some cases, calculation of a(MgO) from the Gibbs-Duhem equation (Kojima et al., 1969; Sakawa et al., 1976; Plante et al., 1992). In all cases, a positive deviation from ideality is reported for a(FeO). Plante et al. used a KEMS method and their Knudsen cell had an iridium liner in a tungsten cup. Measurements were taken over the entire range of compositions from fayalite to forsterite at 1973 K in the molten phase. KEMS measurements of olivine were reported in another study (Piacente et al., 1975). Several dif- ferent Knudsen cells of zirconia, thoria, and rhenium were used in the temperature range 1678–1925 K and rhenium was found to be the most inert. The observed vapor species were Fe, SiO, Mg, and O_2 and partial pressures were reported as a function of temperature.

The calculated pseudo-binary (Fo-Fa) phase diagram is shown in Fig. 1 (a). This shows the classical 'cigar shape', which is in- dicative of a near-ideal solution. Fig. 1 (b) is the calculated phase diagram for the pseudo-binary MgO–'FeO'–SiO_2 system at 1400 K (Fabrichnaya, 1998; Fabrichnaya, 2000; Andersson et al., 2002). The MgO–'FeO'–SiO_2 system has been modeled by several investigators. Saxena et al. (1993) first described the olivine solution as a regular solution with a single, temperature independent solution parame- ter. Fabrichnaya modeled the entire MgO–'FeO'–SiO_2 system with a sublattice model for the solid phases and ionic model for the liquid phase (Fabrichnaya, 1998, 2000). This system has also been mod- eled with a modification of the quasi-chemical model (Wu et al., 1993; Decterov et al., 2002).

The vaporization and condensation kinetics of olivine are im- portant to understand processes in the early solar nebula and have been studied by Nagahara and colleagues (Nagahara et al., 1988; Nagahara et al., 1994; Ozawa and Nagahara, 2000). The results in- dicate the vaporization of olivine is complex. Their results suggest that forsterite and fayalite vaporize congruently (i.e. composition of the starting material remains the same). Condensates consist of olivine, pyroxene, silica and iron, suggesting that the condensation occurs with decomposition.

In this study, we examine near-equilibrium vaporization of olivine in iridium cells with Knudsen effusion mass spectrometry (KEMS). Initial measurements were taken below, through the melt- ing point (solidus) into the two phase region (olivine + liquid), and above the liquidus of the olivine polycrystalline sample. We report the pressures of each vapor constituent over a $Fo_{95}Fa_5$ composition as a function of temperature. Samples were characterized with par- ticular care before and after vaporization. Thermodynamic data are interpreted as both a pseudo-binary and pseudo-ternary. The re- ported vapor pressures are used to calculate thermodynamic activ- ities, which are compared to those from prior measurements and models of this system and related systems. We conclude with a discussion of implications of these measurements for the silicate atmospheres of the hot rocky exoplanets.

2. Experimental methods

2.1. Materials

Natural olivine used in this study is from one of the dunite de- posits on the west coast of Norway and was provided by Miller & Co., Chicago, IL. We used a natural material in this study to measure and understand the mineral olivine. As discussed in the Supplementary Material, we were able to purify this natural olivine to high level and obtain reliable thermodynamic data. The as- received powder sample was annealed in a vacuum furnace at 1700 K for 10 h to eliminate the impurities. After the impurities were removed by heat treatment in vacuum, this sample was ana- lyzed by KEMS below and above its melting point (solidus).

2.2. Knudsen effusion mass spectrometry (KEMS)

Knudsen Effusion Mass Spectrometry was performed using a modified Nuclide-type 12-HT-90 (Nuclide/MAAS/PATCO, formerly of State College, PA) mass spectrometer. The equipment and ex- perimental procedures have been described previously (Drowart and Goldfinger, 1967 ; Kato, 1993 ; Copland and Jacobson, 2010).

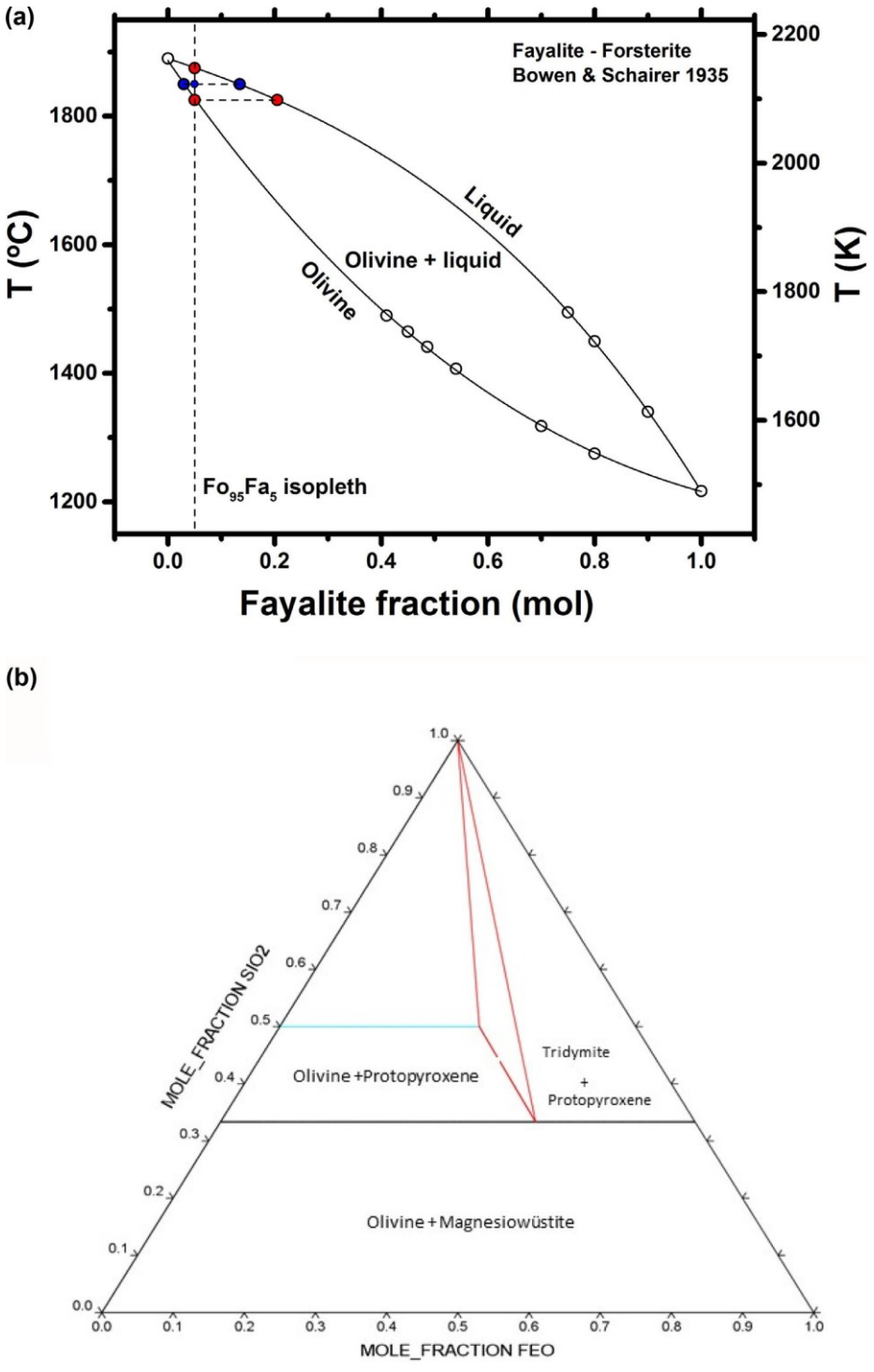

Fig. 1. (a). Calculated pseudo-binary (Fo-Fa) phase diagram (Bowen and Schairer, 1935) (b). Calculated pseudo-ternary MgO–'FeO'–SiO_2 phase diagram.

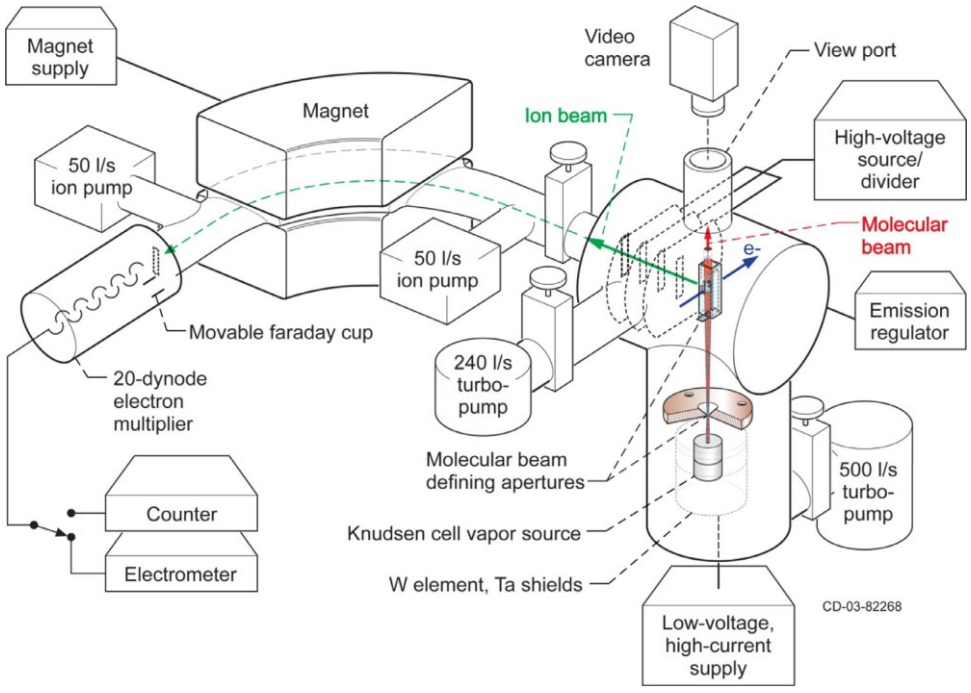

Fig. 2. Knudsen effusion mass spectrometer (Copland and Jacobson, 2010).

The instrument consists of four differentially pumped chambers— Knudsen cell chamber with furnace, ionizer chamber, magnet drift tube, and analyzer chamber. The instrument schematic is shown in Fig. 2 .

After some experimentation (discussed in Supplementary Mate- rial), an iridium cell was selected for this study. This was placed in a graphite support, as iridium is known not to form carbides (Lee and Worrell, 1989). This assembly was supported by a tripod and restively heated with a tantalum heating element in a repeating 'hair-pin' shape. The tantalum heating element and the cell were enclosed in a dense heat shield pack consisting of four inner layers of reflective tungsten and four outer layers of molybdenum. Temperatures above 20 0 0 K were reached with this configuration and were measured with a disappearing-filament-type pyrometer (Mi- crotherm, Pyrometer Instrument Co., Windsor, NJ). Calibration of the instrument and the pyrometer were performed prior to each experiment with an ITS-90 gold standard (Preston-Thomas, 1990) in a graphite cell, either via melting or adjusting the temperature correction for the tabulated enthalpy of vaporization (Hultgren et al., 1973). This procedure allowed temperature measurements to within ±3 K.

The vapor effusing from the cell is directed into the mass spec- trometer. A moveable shutter located between the Knudsen cham- ber and ionization chamber was used to subtract the background contribution from the total signal. For most of the species stud- ied, the background was very small in our instrument. However for SiO(g) at mass-to-charge ratio of 44, CO_2 (g) gave a signifi- cant background and the shutter was essential for measurement. In addition, a liquid nitrogen cold finger placed into the ioniza- tion chamber was used to condense and reduce the background CO_2 gas.

The ionization chamber is located directly above the Knud- sen cell. Ionization is accomplished with 26 or 16.5 eV electrons at a total emission current of 2 mA. The molecular beam from the Knudsen cell, ionizing electron beam, and resultant ion beam are all mutually perpendicular in our instrument. The partial vapor pressures of the ionic species of the samples were calculated through the following relationship (Drowart and Goldfinger, 1967; Copland and Jacobson, 2010).

$$P_i = \frac{k I_i T}{\sigma_i(E)} \quad (2)$$

where P_i (bar) is the partial pressure of the species inside of the cell at absolute temperature T, k is the instrument calibra- tion constant (bar · m^2 · cps^{-1} · K^{-1}) determined from the triple- point plateau of gold at 1337.3 K, I_i (counts per second, cps) is the ion intensity of the species and σ_i (m^2) is the ionization cross section of the species taken from Mann's tabulation of atoms (Mann, 1967) which is a function of ionizing electron energy, E . Mann's values were corrected for the lower electron energies used with the Bonnell Bell Distribution code (Drowart et al., 2005). For molecules, the atomic cross sections are summed and multiplied by 0.75 (Stolyarova et al., 1994). In order to measure both atomic and diatomic oxygen, ionizing electrons with an energy of 16.5 eV were used. This was derived from 12.1 eV (First ionization poten- tial of diatomic oxygen Field and Franklin, 2013) and 5 eV (bond energy of oxygen double bond Pauling, 1960). So as long as the ionizing electron energy is less than 17 eV, we will ionize diatomic oxygen, but not fragment it.

The ion beam is focused with a series of plates near 10 kV and directed into a magnetic analyzer. The proper mass-to-charge ra- tio was set by adjusting the magnetic field. The ions were de- tected with a 20 dynode electron multiplier in a counting config- uration. The use of a non-magnetic ionizer, magnetic analyzer, and ion counting should yield a calibration constant (Eq. (2)) that is independent of mass number.

The instrument was computer controlled and the data ac- quired with NASA Glenn software (Copland et al., 2013). Initially a full mass scan was conducted to determine the major vaporizing species. Species were further identified from their mass-to-charge ratio and appearance potentials. Individual peaks were scanned six times for adequate statistics.

The component thermodynamic activities in the olivine system are calculated through the measurements of the vapor pressures of the species in equilibria with olivine (see the chemical equations below). For the activity calculations, it is assumed that the olivine system is a three component system of 'FeO' (wüstite), MgO (peri- clase), SiO_2 (high cristobalite).

$$FeO(olivine) = Fe(g) + ½\ O_2(g) \quad (3)$$

$$MgO(olivine) = Mg(g) + ½\ O_2(g) \quad (4)$$

$$SiO_2(olivine) = SiO(g) + ½\ O_2(g) \quad (5)$$

Taking as an example SiO_2. The equilibrium constant of this re- action can be written as given below where *f(i)* is the fugacity of species *i* :

$$K = \frac{f(SiO, \text{soln})\,[f(O_2, \text{soln})]^{1/2}}{a(SiO_2)} \quad (6)$$

This can be compared to the calculated value for pure 'SiO_2':

$$K = f^o(SiO)\,[f^o(O_2)]^{1/2} \quad (7)$$

Equating these two expressions and assuming for these low pressures, partial pressure is equal to fugacity, leads to:

$$a(SiO_2) = \frac{P(SiO, \text{soln})\,[P(O_2, \text{soln})]^{1/2}}{P^o(SiO)\,[P^o(O_2)]^{1/2}} = \frac{Keq, \text{soln}}{Keq, \text{pure}} \quad (8)$$

Similar expressions can be derived for each component oxide. The advantage of this procedure is that the instrument constant, k, and ionization cross section, $\sigma_i(E)$, cancel and hence this source of error is eliminated. However, it is essential to mass spectrometri- cally measure the equilibrium constants for the pure materials as part of the study. This is the standard method for measuring ac- tivities in oxide solutions (Stolyarova et al., 1994; Copland and Ja- cobson, 2001). For MgO and SiO_2, it was possible to measure both the metal containing species and oxygen. Since stoichiometric FeO does not exist, we used Fe-rich FeO. Wüstite (FeO) coexists with Fe at this Fe-rich boundary compositions (Wriedt, 1991) which al- lowed the KEMS measurements of the partial vapor pressures of Fe(g). This resulted in oxygen pressures below the instrument's levels of detection. Thus oxygen pressures were calculated from their stoichiometric relationship to the measured partial pressure of Fe(g). The dependence of the log of activity on inverse temper- ature gave the partial molar enthalpy for each component.

We used a single Knudsen cell furnace (Copland and Jacobson, 2010) configuration, which required a different run for each refer- ence material and the solid solution. Before each run, a calibration run was conducted with Au, to determine the calibration instru- ment constant k (Eq. (2)). We found the calibration constant to be constant between runs.

3. Results

3.1. Elemental and phase composition of the samples

The as-received olivine sample contained the secondary phases enstatite (6.4 ± 0.1%), clinochlore (3.5 ± 0.2%), sapphirine (0.80 ± 0.06%) and quartz (0.79 ± 0.04%) as impurities (Supplemen- tary Material, Figure S1). This sample was heat treated at 1700 K for 10 h in vacuum to eliminate the impurities and later it was used in the KEMS vaporization experiments. Powder X-ray diffrac- tograms (Supplementary Material) of the samples before and af- ter the KEMS experiments performed below the melting point (solidus) of olivine confirm formation of a single crystalline phase in these samples. However, 15.1 ± 0.3% protoenstatite was found in the sample heated above the solidus. The lattice parameters of the olivine are consistent with pure forsterite but electron probe microanalysis found trace amounts of FeO that correspond to $Fo_{99.8}Fa_{0.2}$ composition for the olivine and $En_{99.8}Fs_{0.2}$ for the py- roxene. The crystallite sizes calculated using a whole pattern fitting procedure (Rietveld refinement) of the sample diminished from 453 ± 8 nm to 329 ± 7 nm after the KEMS experiment (below melt- ing point or solidus). Powder X-ray diffractograms of the reference samples FeO/Fe, MgO and SiO_2 after the KEMS experiments con- firmed that they are single crystalline phases. The chemical com- position of the samples before and after KEMS that were mea- sured by inductively coupled plasma–optical emission spectroscopy (ICP-OES) and electron probe microanalysis (EPMA) is given in Table 1 . The chemical composition of the samples in Table 1 is given for the contents of elements, oxides, and fosterite/fayalite since olivine constituents have different terminologies in differ- ent fields of science. Before and after KEMS, the fosterite content remained the same within experimental uncertainties (95 ± 5 wt. % - before, 96 ± 5 wt. % - after) and the fayalite content dimin- ished 1.0 ± 0.3 wt. %. This wt. % decrease of the fayalite content translates to a decrease of 0.7 ± 0.2 wt. % of Fe and 1.1 ± 0.4 wt. % of FeO. We use $Fo_{95}Fa_5$ throughout the manuscript since this was the measured composition before KEMS and it has only de- creased 1.0 ± 0.3 wt. % of its fayalite content. Above the melting point or solidus, the fayalite content diminished to 0.21 ± 0.01 wt. % (0.16 ± 0.01 wt. % of Fe or 0.18 ± 0.01 wt. % of FeO). Considering the composition of the sample before KEMS, olivine almost lost all of its iron content (4.7 ± 0.2 wt. % of fayalite, 3.4 ± 0.2 wt. % of Fe and 4.9 ± 0.4 wt. % of FeO.

Table 1
Chemical composition of the olivine powder samples before and after KEMS.

Element/Oxide	Weight (%)[a]			
	Olivine as-received	Olivine		
			After KEMS Below melting	After KEMS[c] Above melting
Mg	30(2)	30(2)	32(2)	33.1(6)
Fe	5.0(3)	3.6(2)	2.9(1)	0.16(1)
Si	20(1)	17.0(9)	17.2(9)	27.9(5)
		Before KEMS		
MgO	50(4)	55(4)	57(4)	48(1)
FeO	6.5(5)	5.1(4)	4.0(2)	0.18(1)
SiO_2	43(3)	40(3)	39(3)	52(1)
Mole (%)[b]				
Mg, forsterite	93(5)	95(5)	96(5)	100(2)
Fe, fayalite	6.7(3)	4.9(2)	3.9(2)	0.21(1)

[a] Uncertainties of the analyses are given in parentheses. [b] Mg, forsterite mole (%) = Weight% $_{Mg}$/(24.305 total mol) 100. Fe, fayalite mole (%) = Weight% $_{Mg}$/(55.845 total mol) 100. Total mol = (Weight% $_{Fe}$/55.845) + (Weightt% $_{Mg}$/24.305). Total sum of the Al, Ca, Co, Mn and Ni contents are less than 0.5 wt %. [c] EPMA. According to X-ray elemental mapping, iron is distributed in the fosterite rich olivine and protoenstatite phases.

3.2. Vapor composition

The ionic species detected by KEMS in the vapor phase of the olivine sample between 1751–2225 K are listed in Table 2 . Appear- ance potentials were measured via extrapolation of the linear seg- ment of the ionization efficiency curves and these are statistically indistinguishable to those reported earlier (Levin and Lias et al. 1982). The neutral precursors of these ions were identified from their mass-to-charge ratio and their appearance potentials. The

Table 2
Vapor species of the olivine sample detected by KEMS and their appearance potentials (eV).

Vapor Species	Appearance potential (eV)	
	*This work	Levin et al. (1982)
Mg^+	7.46	8.18 ± 1.81
	7.63	7.7 ± 0.20
Fe^+		

FeO +	8.25 ± 1.5	8.71 ± 0.10
SiO +	10.60 ± 1.83	10.53 ± 0.02
O +	14.9 ± 1.93	14.0 ± 0.5
O_2 +	17.22 ± 2.88	18.69 ± 0.04

* Extra digit is retained to prevent round-off errors.

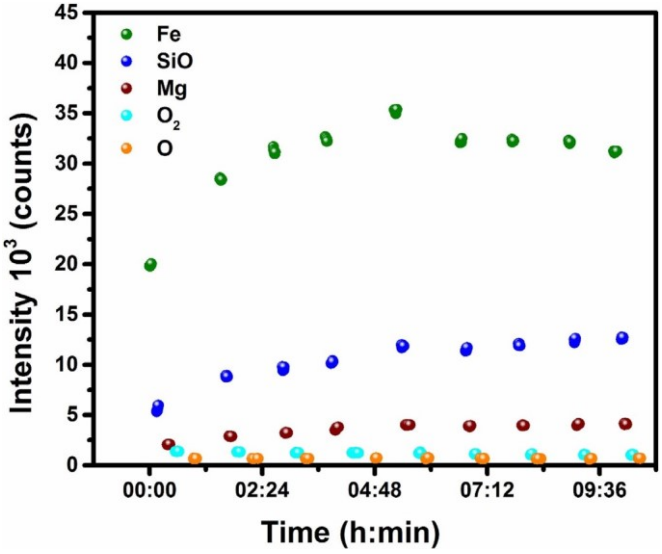

Fig. 3. Dependence of the ion intensities of the vapor species of olivine over time at 1890 K.

primary vapor species above olivine are thus Fe(g), Mg(g), SiO(g), O_2(g), and O(g). No major breaks were observed in the ionization curves, indicating that fragmentation of the polyatomic species did not occur during the ionization process. As discussed previously, O_2 (g) does fragment to O(g) at higher ionizing electron energies and low electron energies were used to prevent this.

3.3. Time to equilibration

KEMS equilibrium studies were conducted after isothermal heating (Fig. 3) when the ion intensities of the vapor species of olivine were constant with time. The ion intensities of iron and silicon oxide increased from 20×10^3 cps to approximately 30×10^3 cps and from 5×10^3 cps to approximately 10×10^3 cps in the initial 5 h of the isothermal experiment, respectively. Although the ion intensities of iron and silicon monoxide changed drastis- cally in the initial stage of vaporization, the ion intensities of mag- nesium, and molecular and atomic oxygen were apparently con- stant with time during the whole isothermal experiment. This is see in the data points on the isothermal graph in Fig. 3 , where the values of the ion intensies of these species changed slightly over time. Such small fluctuations of the ion intesities of the va- por species are not expected to influence the thermodynamic data above the experimental uncertainties.

The attainment of equilibrium in a Knudsen cell is a critical issue in Knudsen effusion studies (Cater, 1979). Dohmen et al. (1998) have carefully examined the system Fe/olivine and used a Knudsen cell to monitor reaction progress. They discuss preferen- tial loss of Mg(g) from the olivine and compositional zoning within the grains. Although their system is compositionally different from ours, such processes must be considered in our system as well. We believe that equilibrium in our cell is reached due to (1) Our cell was kept at 1890 K for > 10 h (2) The vapor pressures were con- stant within experimental error as discussed above (3) A plot of the logarithm of vapor vs inverse temperature was linear.

Table 3
Partial molar enthalpies of MgO, 'FeO', and SiO_2 as determined from ac- tivity dependence on inverse temperature.

Component	This study	Calculated from Fabrichnaya database
MgO	[redacted]	[redacted]
'FeO'	–	70.73
SiO_2	98.0 ± 3.6	

3.4. Thermodynamic properties

3.4.1. Reference materials

The data for vapor pressures of the species above the three ref- erence materials— SiO_2 , FeO and MgO—are shown in Fig. 4 . We used 'FeO' with excess Fe to fix the composition of 'FeO'. As noted, the $P(O_2)$ in this case is below the limits of detectability and the $P(O_2)$ used in reaction (2) was calculated from the measured P(Fe) and the data in FactSage (Bale et al., 2002). These in turn were used to calculate their equilibrium constants for reactions (3–5), which are also shown in Fig. 4 . For MgO and SiO_2 the data taken here were reasonably close to published equilibrium data from the tables (Chekhovskoi et al., 1993; Bale et al., 2002). Data were used only where (1) the ratio of the partial pressures of the metal-bearing and diatomic oxygen were close to that predicted from equilibrium calculations and (2) the calculated equibrium between diatomic and monatomic oxygen was close to that predicted. Dif- ferences are due to uncertainty in the ionization cross sections (Eq. (2)) and small deviations from equilibrium encountered in a Knud- sen cell. This underscores the need for running reference materials under the same experimental conditions as the solid solution un- der examination.

3.4.2. Olivine

Initial measurements were taken through the melting point (solidus) into the two phase region, and above the liquids as shown in Fig. 5 . Near the solidus there were significant discon- tinuities in the measured ion intensities. These suggest the onset of melting is near 2050 K for $Fo_{95}Fa_5$, which is consistent with the phase diagram for forsterite-fayalite, as shown in Fig. 1 (a) (Bowen and Schairer, 1935). Our chemical analysis indicates that after melting there is a rapid loss of Fe, which is also consistent with these changes in partial pressures on melting.

Mysen and Kushiro (1988) studied forsterite vaporization using Knudsen effusion weight loss measurements. They also noticed a large discontinuity at ~1700 °C (~1973 K) where liquid formed in their experiments, about 190 ° below the forsterite melting point of 1890 °C (2163 K). The large melting point depression may be due to impurities in their sample (e.g., see pp. 1953–1954 of Nagahara et al., 1994). Mysen and Kushiro's (1988) data were much more scat- tered above than below the melting point, as seen in their Table 2 . Vapor pressure measurements below the melting point are shown in Fig. 6 . Using the procedure of equilibrium constant ratios, as dis- cussed previously, thermodynamic activities are derived as a func- tion of inverse temperature and shown in Fig. 7 . Partial molar en- thalpies are determined from the slope of this plot and listed in Table 3 .

4. Discussion

4.1. Enthalpy and entropy of vaporization for olivine

Treating the system as a Fo-Fa pseudo-binary, we computed partial molar enthalpies of vaporization of fayalite and forsterite from the measured Fe and Mg partial vapor pressures over the $Fo_{95}Fa_{0.05}$ sample. Our treatment follows that of Nagahara et al. (1994) and Dohmen et al. (1998) . At chemical equilibrium between olivine and vapor the chemical potentials of forsterite (μ_{Fo}) and fayalite (μ_{Fa}) are equal in the two coexisting phases. This is ex- pressed by the equations:

$$Fa\,(\text{olivine}) = Fa\,(\text{gas}) \quad (9)$$

$$\mu_{Fa}(\text{olivine}) = \mu_{Fa}(\text{gas}) \quad (10)$$

$$Fo(\text{olivine}) = Fo(\text{gas}) \quad (11)$$

$$\mu_{Fo}(\text{olivine}) = \mu_{Fo}(\text{gas}) \quad (12)$$

The reaction isotherms for the two vaporization reactions are

$$\mu_{Fa}(\text{gas}) - \mu_{Fa}(\text{olivine}) = K_{Fa} \quad (13)$$

$$\mu_{Fo}(\text{gas}) - \mu_{Fo}(\text{olivine}) = K_{Fo} \quad (14)$$

The equilibrium constants K_i (where i = Fa or Fo) are given by

$$K_{Fa} = P_{Fa(gas)} - a_{Fa(olivine)} \quad XP_{FFaa} = XP_{FFea} \quad (15)$$

$$K_{Fo} = P_{Fo(gas)} - a_{Fo(olivine)} \quad XP_{FFoo} \sim XP_{FFoo} = PX_{MgFo} \quad (16)$$

The equilibrium constant expressions above assume ideality for olivine and gas (i.e., fugacity f = partial pressure P and thermody- namic activity a = mole fraction X). An ideal gas is a good assump- tion at the high temperatures and low total pressures in the KEMS experiments.

We initially assume ideal solid solution of fayalite and forsterite in olivine and then explore the effects of non-ideality, which are small (e.g., Dachs and Geiger, 2007 ; von Seckendorff and O'Neill, 1993 ; Wiser and Wood, 1991 ; Nafziger and Muan, 1967). To first

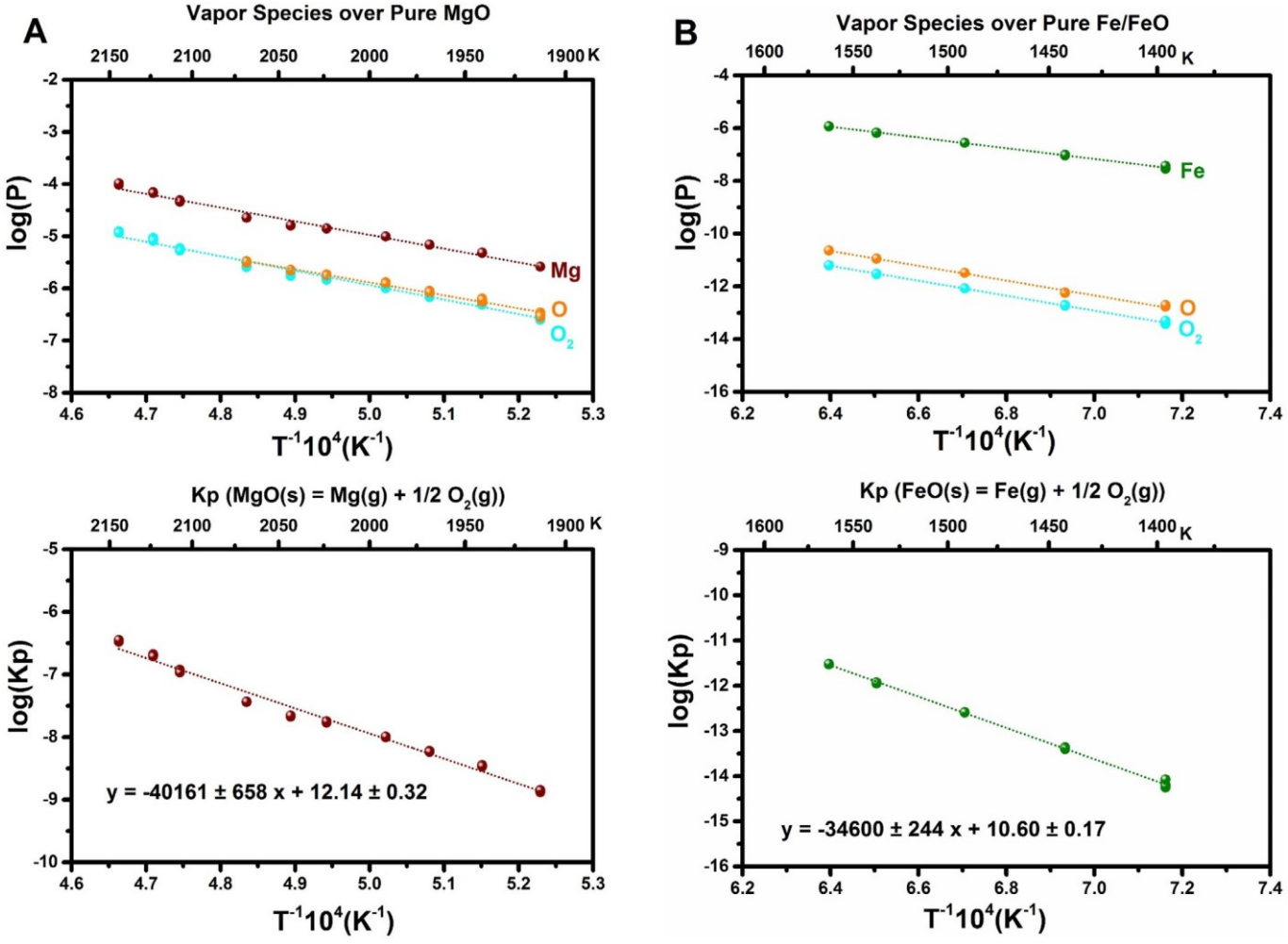

Fig. 4. Temperature dependence of the ion intensity ratios of the vapor species ab ove the reference materials—(A) MgO, (B) Fe/FeO, and (C) S iO 2 . Note that for Fe/FeO the oxygen partial pressures are calculated. Equilibrium constants are calculated for each reaction (3-5) and also plotted.

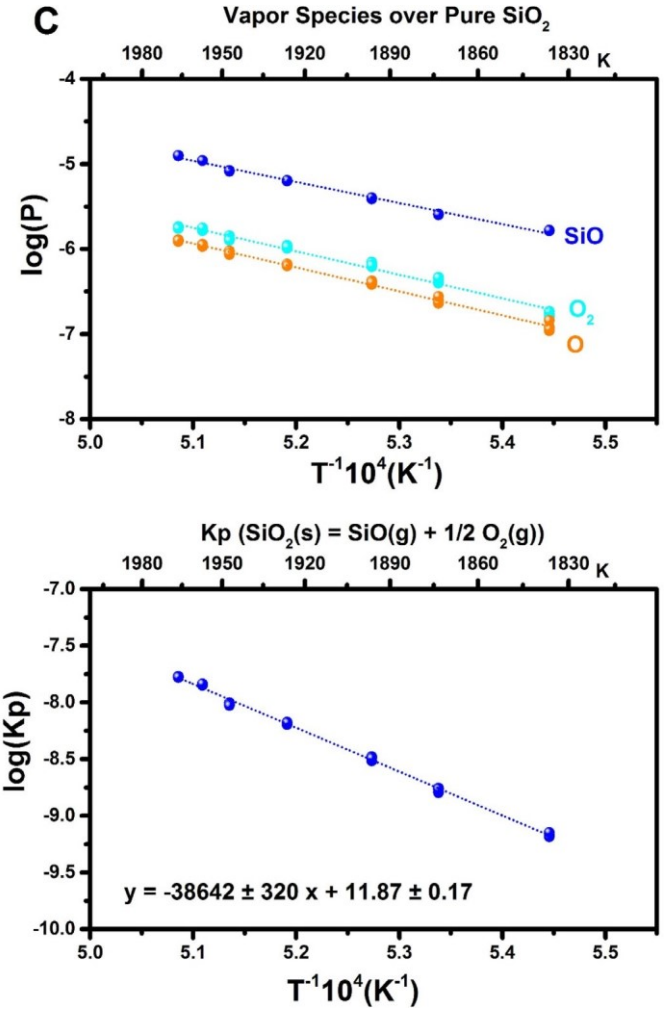

Fig. 4. Continued

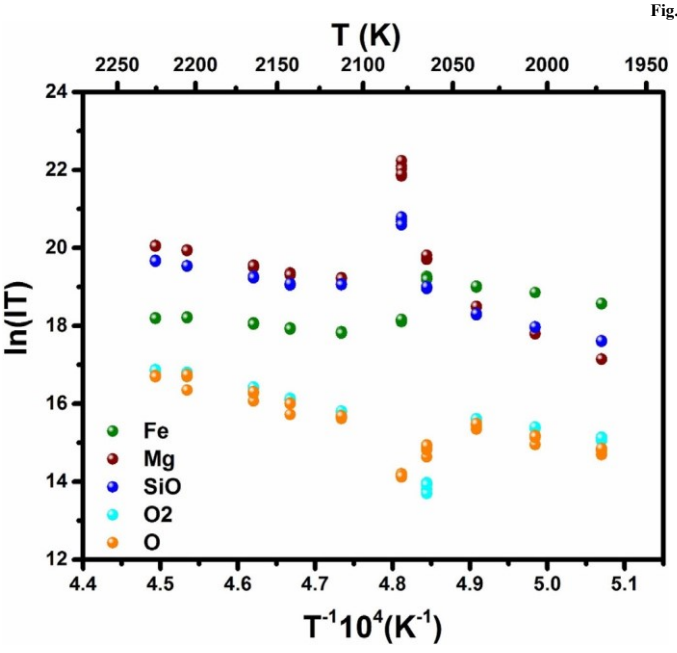

Fig. 5. Temperature dependence of the ion intensities for each species through the melting point. On-set of melting is ~2050 K. Energy of ionizing electrons was 26 eV **Table 4**
Thermochemical data for olivine vaporization.

Component H_{vap} (kJ/mol)	S_{vap} (J/K ·mol)	Reference
Forsterite (solid)	585 ± 4	183 ± 2	
regular Fo_{95} Fa_5	585 ± 4	183 ± 2	This work
ideal Fo_{95} Fa_5	548 ± 13	233 ± 13	This work
ideal Fo_{90} Fa_{10}	543 ± 33	169 ± 21	Piacente et al. (1975)
Fo_{100}	640 ± 36	210 ± 54	Nagahara et al. (1994)
Fo_{100}	431 ± 3	156 ± 2	Mysen and Kushiro (1988)
Fayalite (liquid)	428 ± 3	153 ± 2	This work
regular Fo_{95} Fa_5	410 ± 15	179 ± 14	This work
ideal Fo_{95} Fa_5	412 ± 7	139 ± 4	Piacente et al. (1975)
ideal Fo_{90} Fa_{10}			Nagahara et al. (1994)
Fa_{100}			

approximation, the temperature dependence of the K values for the vaporization reactions are given by

$$\ln K_{Fa} = \frac{P(Fe)}{R} = \ln - \frac{S_{vF\ apa}}{R} \frac{H_{vF\ apa}}{RT} \quad (17)$$

$$\ln K_{Fo} = \frac{P(Mg)}{R} = \ln - \frac{S_{vF\ apo}}{R} \frac{H_{vF\ apo}}{RT} \quad (18)$$

The H_{vap} and S_{vap} values for forsterite and fayalite calcu- lated assuming ideal solid solution in olivine are given in Table 4 . Here R and T are the gas constant and absolute temperature,

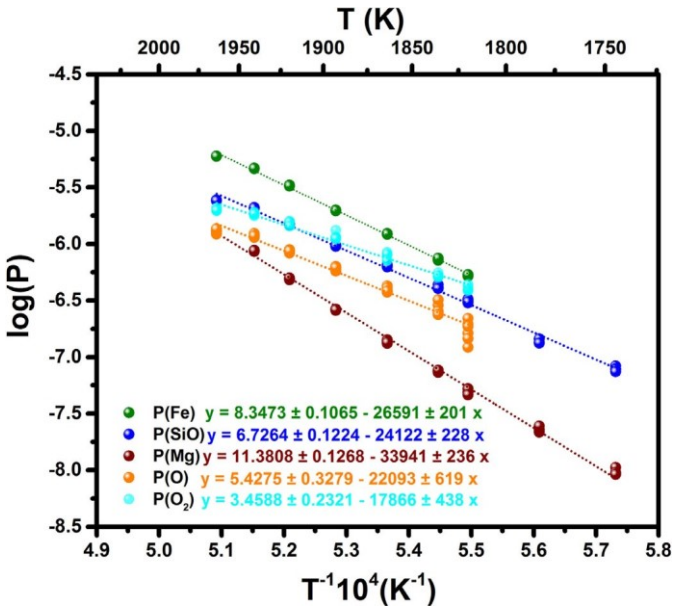

Fig. 6. Dependence of the partial pressures of the species above olivine with in- verse temperature for olivine (Fo_{95} Fa_5). Energy of ionizing electron 16.5 eV.

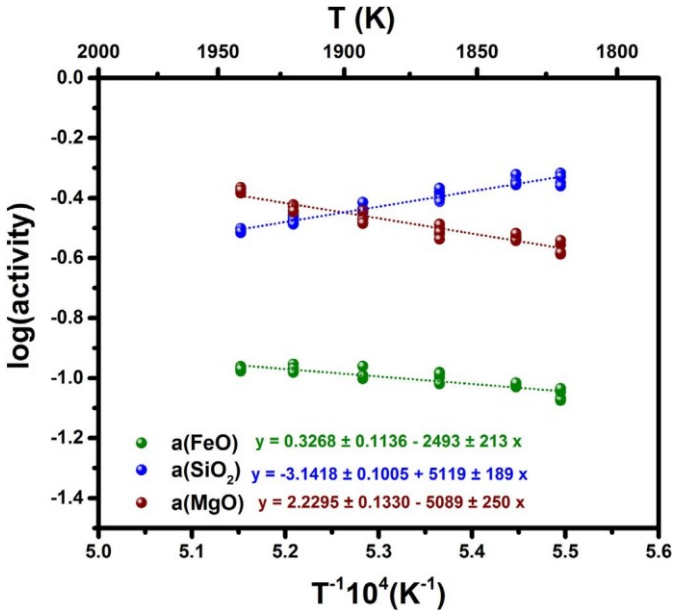

Fig. 7. Thermodynamic activities for FeO, MgO, and SiO_2 in olivine as a function of inverse temperature.

respectively. There is fairly good agreement with the prior work of Nagahara et al. (1994) on pure forsterite and Piacente et al. (1975) on a Fo-rich olivine (Fo_{90} Fa_{10}) similar in composition to our sample. However Mysen and Kushiro (1988) derived a much higher H_{vap} for their forsterite sample. As mentioned earlier their sample also melted 190 K below the accepted value (2163 K) for forsterite and may have contained impurities, causing a melting point depressions. Our fayalite (liquid) H_{vap} and S_{vap} values also show good agreement with those of Nagahara et al. (1994) and Piacente et al. (1975) . The vapor pressures (P_{vap}) of pure forsterite and pure fayalite were calculated at their triple points (2163 K and 1490 K, respectively) from our measured Mg and Fe partial pres-

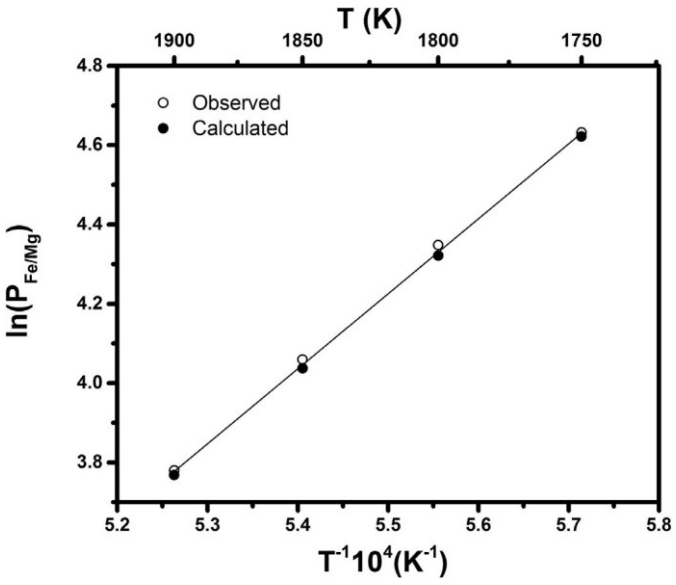

Fig. 8. Plot of pressure ratios of Fe to Mg versus inverse temperature.

sures over Fo_{95} Fa_5 olivine assuming ideal solid solution:

[redacted] $P(Mg)$ 70,364 ± 418 (19)

[redacted] $P(Fe)$ 51,452 ± 306 (20)

The calculations give P 2.6 × [redacted] 10^{-5} bar at the forsterite triple point versus 5.2 × 10^{-} bar determined by Nagahara et al. (1994) and P_{vap} = 14 × 10^{-8} bar at the fayalite triple point versus 6.3 × 10^{-8} bar from Nagahara et al. (1994) . Agreement is slightly better for forsterite than fayalite but is within a factor of 2.2 in both cases. Fig. 8 is a plot of ln *(P(Fe)/P(Mg))* versus inverse temperature. The close agreement between the observed and calculated values shows the near ideality of olivine as a pseudo-binary sys- tem.

As mentioned in the Introduction, the forsterite–fayalite solid solution has small positive deviations from ideality. There is no sta- tistically significant excess entropy of mixing (Dachs and Geiger, 2007), so a symmetric regular solution model with one param- eter, as recommended by many groups (e.g., Dachs and Geiger, 2007 ; von Seckendorff and O'Neill, 1993 ; Wiser and Wood, 1991 ; Kitayama and Katsura, 1968 ; Larimer, 1968 ; Nafziger and Muan, 1967) is sufficient for describing the small amounts of non-ideality. The Mg^{2+} and Fe^{2+} cations can be distributed on the M1 and M2 octahedral sites in olivine (Muan, 1967 ; Nafziger and Muan, 1967) so the equations for the activity coefficients of forsterite and fay- alite are written in terms of one half formula unit, e.g. $MgSi_{0.5}O_2$ (= ½ Mg_2SiO_4) and $FeSi_{0.5}O_2$ (= ½ Fe_2SiO_4). We used the equations

$$RT\ln(\gamma_{FeSi_{.5}O_2}) = RT\ln(\gamma_{Fa}) = W_G X_{MgSi_{.5}O_2}^2 \quad (21)$$

[redacted] RT $_{MgSi_{.5}O_2}$ Fo $W_G X_{Fe Si_{.5}O_2}^2$ (22)

Here γ_i is the activity coefficient of component i. We use a Mar- gules parameter $W_G = 3700$ J mol^{-1} (von Seckendorff and O'Neill, 1993 ; Wiser and Wood, 1991). For the $Fo_{95}Fa_5$ olivine over the 1750–2050 K range, this regular solution model gives

$$ln(\gamma_{Fa}) = \frac{402}{T}; \gamma_{Fa} = 1.26 \text{ to } 1.22 \quad (23)$$

[redacted] (24)

In other words the $Fo_{95}Fa_5$ olivine is ideal within 26%, and Table 4 shows the H_{vap} and S_{vap} values for the regular solu- tion model are very similar to those assuming ideal solid solution.

Table 1 shows the composition of the olivine changed by about 1 mol% over the course of the KEMS experiments from $Fo_{95}Fa_5$ to $Fo_{96}Fa_4$, and it is possible this change could have affected the H_{vap} and S_{vap} values computed from our work. But the effect if any seems minor because of the good agreement of our calculated vapor pressures at the fayalite and forsterite triple points with those reported by Nagahara et al. (1994) and with their H_{vap} and S_{vap} values.

4.2. Fractional vaporization of Fe and Mg from olivine

In their pioneering study, Nagahara et al. (1988) showed frac- tional vaporization of olivine in their Knudsen effusion weight loss experiments from electron microprobe analyses of the vaporized residual olivine. But they did not measure the partial pressures of the evaporating gas species. Ozawa and Nagahara (20 0 0) studied the kinetics of fractional vaporization of $Fo_{92}Fa_8$ olivine at 1414 °C (1687 K) but did not measure gas chemistry or study the temper- ature dependence. Fig. 8 shows that the measured Fe/Mg partial pressure ratio in the saturated vapor in equilibrium with olivine is larger than the Fa/Fo molar ratio in olivine,

$$\frac{(Fe/Mg)_{gas}}{(Fe/Mg)_{olv}} > 1 \quad (25)$$

The fractional vaporization of Fe and Mg is a consequence of the different Gibbs energies of vaporization of the fayalite and forsterite components in solid solution in olivine. We can show this by rearranging the equations for K_{Fa} and K_{Fo} to solve for the Fe/Mg ratio in the gas:

[redacted] $\frac{Fe}{a_{Fa}}$

$-G^{o}_{vap}(Fo)/RT$

$$ln\,Mg_{gas} = ln\,a_{Fo\,Olv} - ln - G_{ovap}(\ )/ \quad (26)$$

The G^{o}_{vap} values for forsterite and fayalite are given by

$$G_{ovap} = H_{vo\,ap} - TS_{vo\,ap} \quad (27)$$

The values for the enthalpy and entropy of vaporization are in Table 4 . Agreement between our data and the literature data is good for fayalite. For forsterite, there is about 7% difference be- tween our data and that of Piacente et al. (1975) and Nagahara et al. (1994) and about 9.4% difference between our data and that of Mysen and Kushiro (1988) . Nagahara et al. (1994) points out that the larger values obtained by Mysen and Kushiro (1988) are pos- sibly due to their weight loss measurement including the capsule, cap, and wire in addition to the sample, which could overestimate the weight loss. Differences could also be attributed to possible cell reactions—as discussed in the Supplementary Material, only Ir showed some degree of inertness to olivine.

We reach exactly the same conclusion if we treat olivine vapor- ization as an exchange reaction as done by Dohmen et al. (1998) . In this case

$$MgSi_{.5}O_2(Fo) + Fe(g) = FeSi_{.5}O_2(Fa) + Mg(g) \quad (28)$$

At chemical equilibrium,

$$\mu_{Mg(g)} + \mu_{Fa} = \mu_{Fe(g)} + \mu_{Fo} \quad (29)$$

The reaction isotherm for the exchange reaction is

[redacted]

$+RT\,ln\,K_{ex}$ (30)

The equilibrium constant (K_{ex}) for the exchange reaction is

K_{ext} [redacted]

$-\ Mg(g)\quad Fa - Fe(g) - Fo\ ff_{MgFe}a\,a_{FF\,oa} \sim PP_{MgFe}$

$XX_{FF\,oa}$

(31)

The relationship between Fa and Fo in olivine and Fe and Mg in the gas is thus

$$\frac{a_{Fa}}{} = K_{ex} \cdot \sim \overline{=K_{ex}} \cdot \frac{X_{Fa}}{} \frac{P_{Fe}}{} \quad (32)\ a_{Fo} f_{Mg} X_{Fo} P_{Mg}$$

The right most part of this equation is the approximate expres- sion derived by Dohmen et al. (1998) and shows the equality of our two treatments.

In principle we could use the Fe/Mg ratio in the gas to com- pute the ratio of G^{o}_{vap} values and if the value for one endmember were known accurately, then the other could be computed from the KEMS data for the olivine. This method can be used to compute G^{o}_{vap} for minor components dissolved in olivine such as $CaSi_{0.5}O_2$, $NiSi_{0.5}O_2$, $MnSi_{0.5}O_2$, and $CoSi_{0.5}O_2$ but it has not been done to our knowledge.

Other binary solid solutions with cigar-shaped phase di- agrams should fractionate the more and less volatile end members during vaporization. For example, the solid solu- tions of fayalite–tephroite (Mn_2SiO_4), forsterite–tephroite, Ni_2SiO_4–forsterite, Co_2SiO_4–forsterite, and so on, should have this behav- ior. The albite ($NaAlSi_3O_8$)–anorthite ($CaAl_2Si_2O_8$) phase diagram for plagioclase feldspar (Bowen, 1913) is probably the most well- known cigar-shaped phase diagram in mineralogy and it shows fractional vaporization of Ca and Na (Nagahara and Kushiro, 1989 ; Nagahara, 1990 ; Nagahara et al., 1993). The Ca-rich vaporiza- tion residues and Na-rich vapor condensates show complementary compositions (e.g., Fig. 7 of Nagahara and Kushiro, 1989). They did also Knudsen effusion weight loss measurements but the partial pressures of the different evaporating gases were not measured.

4.3. Olivine as a pseudo-ternary and comparison to assessments

As discussed, olivine can also be regarded a pseudo-ternary of MgO–'FeO'–SiO_2. This is particularly important as the reported vapor pressures originate from each of these three components. These vapor pressures lead to thermodynamic activities of these components. Our data can then be compared to recent thermody- namic assessments of the MgO–'FeO'–SiO_2 system by Fabrichnaya and colleagues (Fabrichnaya, 1998 ; Andersson et al., 2002), to sup- port the consistency of both our measurements and their thermo- dynamic assessment. Their database was constructed with all avail- able thermodynamic and phase data at the time of the assessment and provides a self-consistent thermodynamic description of this system. A comparison of the data from this

study to this assess- ment should indicate if our data is consistent with previous mea- surements and also allows inferences about the exact phase com- position of the olivine. It also should suggest improvements for fu- ture assessments and experiments.

Ideally activity measurements and calculations should be con- ducted in the two phase regions of the pseudo-ternary (Fig. 1), i.e. olivine + protopyroxene, olivine + liquid or olivine + magne- siowüstite. The olivine line in Fig. 1 (b) necessarily has an activity gradient across it. Fig. 9 (a) and (b) are calculations of component activities in these regions using ThermoCalc (Andersson, 2002). Fig. 9 (a) for the olivine + proto-pyroxene and olivine + liquid region was calculated with the olivine composition used here and a lit- tle excess silica. The compositional input was thus x(MgO) = 0.33,

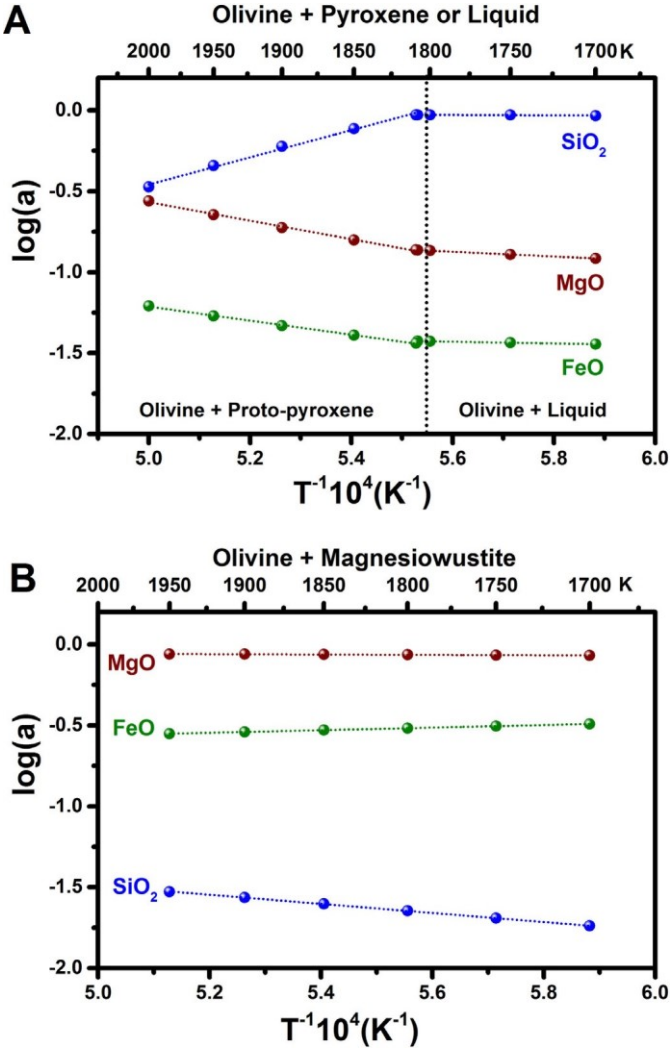

Fig. 9. Calculations of component activities in (Fo $_{95}$ Fa $_{5}$) for (A) olivine + protoprox- ene or liquid and (B) olivine + magnesiowüstite using the database of Fabrichnaya (1998).

x(FeO) = 0.03, x(Fe) = 1 × 10 $^{-5}$, and x(SiO $_{2}$) = 0.34. Fig. 9 (b) for the olivine + magnesiowüstite was calculated with the olivine compo- sition used here and a little excess MgO. In this case the composi- tional input was x(MgO) = 0.63, x(FeO) = 0.03, x(Fe) = 1 × 10 $^{-5}$, and x(SiO $_{2}$) = 0.34. It should be noted that in these two phase regions in a three component system, activity would vary with composi- tion. Since we do not know the composition with extreme preci- sion, these input compositions approximate the analyzed compo- sitions. Thus the calculated values of activities and partial molar enthalpies would not be expected to be identical to our measure- ments. However, they should follow the same trends as our mea- surements, which was indeed observed.

As discussed, the material in our Knudsen cell was shown via XRD to be pure olivine. However the data in Fig. 7 are close to the calculations in Fig. 9 (a) for the excess silica olivine, which equili- brates to olivine + liquid. Our measurements indicate a high silica activity. The equilibrium calculations indicate a small amount of liquid (x(liquid) ~0.04). This may be amorphous on cooling and/or be too small an amount to detect from XRD.

Table 3 compares the measured partial molar enthalpies of each component to those calculated from the database discussed above. Although the measurements and the model show the same trends, agreement between our measurements and the database of Fabrichnaya (1998) is only approximate for the partial molar en-

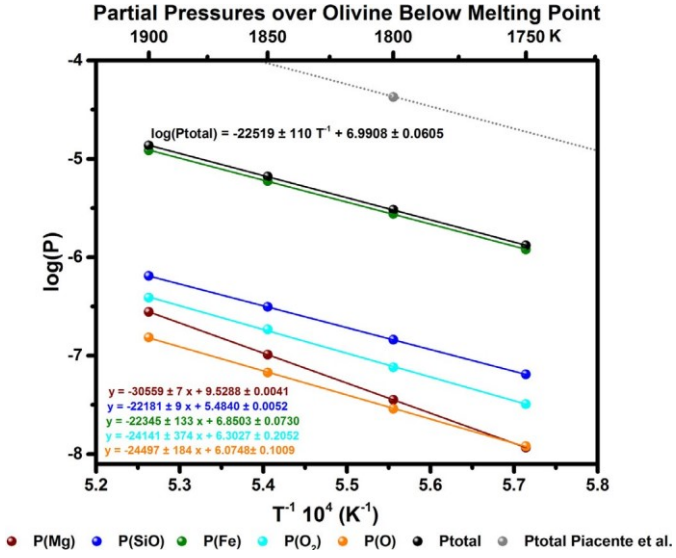

Fig. 10. Total vapor pressure over Fo $_{95}$ Fa $_{5}$ below melting point.

thalpy of SiO $_{2}$ and FeO and there is some disagreement for the partial molar enthalpy of MgO. Some of this can be attributed to compositional differences, as is discussed. However further studies are necessary in well-defined two phase regions to resolve these discrepancies.

4.4. Olivine vapor pressure equation

The total vapor pressure (P $_{T}$) above olivine of composition Fo $_{95}$ Fa $_{5}$ was calculated by modifying the tabulated vapor pressures for MgO, Fe-rich FeO, and SiO $_{2}$ by their measured activities in Fig. 7 . The tabulated vapor pressures were taken from the FactSage code and databases (Bale et al., 2002). The derived vapor pressure equation is

$$logP_T(bar) = 6.9908(\pm 0.0605) - \frac{22,519(\pm 110)}{T} \quad (33)$$

This equation gives a total vapor pressure of ~7 × 10 $^{-6}$ bars at 1850 K (see Fig. 10).

For comparison, the total vapor pressure for the Fo $_{90}$ Fa $_{10}$ olivine studied by Piacente et al. (1975) is ~1 × 10 $^{-4}$ bars at the same temperature, over 10 times larger. This could be due to the higher fayalite content of their olivine (unlikely) or it could be due to is- sues such as the choice of cross sections in the conversion of ion intensity to vapor pressures (Eq. (2)). Their observations are similar to ours otherwise–they obtain the same relative volatility sequence Fe > SiO > O $_{2}$ > Mg and their data give similar H $_{vap}$ and S $_{vap}$ values for forsterite and fayalite, as discussed above. But their va- por pressure is about 10 times larger over the temperature range studied (see Fig. 10) and the cause is unknown.

4.5. FeO gas

Another similarity between our results and those of Piacente et al. (1975) is the absence of FeO (g). Thermodynamic cal- culations using JANAF data predict FeO/Fe ratios ~0.1 in the saturated vapor over olivine which is not observed. Clearly there is a discrepancy between our observations and those of Piacente et al. (1975) as compared to the dissociation en- ergy of ~414 kJ mol $^{-1}$ (based on spectroscopic measurements) adopted by JANAF in 1966. Since 1966, there are several more recent measurements of the FeO dissociation energy that give lower values, e.g., 389 ± 13 kJ mol $^{-1}$ (Murad, 1980), 401 ± 8 kJ mol $^{-1}$ (Smoes and Drowart, 1984), 403 ± 1 kJ mol $^{-1}$ (Chestakov et al., 2005), 405 ± 13 kJ mol $^{-1}$ (Hildenbrand, 1975), and 406 ± 13 kJ mol $^{-1}$ (Balducci et al. 1971). More work is necessary to resolve this discrepancy.

4.6. Molten olivine vaporization

Fig. 1 (a) shows the phase diagram for the forsterite (Mg_2SiO_4)– fayalite (Fe_2SiO_4) binary determined by Bowen and Schairer (1935) . In this diagram, the hollow circles are the points measured by Bowen and Schairer (1935) and Bowen and Anderson (1914) for forsterite, and Bowen and Schairer (1932) for fayalite. The vertical dashed line shows the composition of our olivine sample $Fo_{95}Fa_5$ and the red dots are the expected solidus (1825 °C) and liquidus temperatures (1875 °C) from the phase diagram. As mentioned ear- lier, we observed melting at ~2050 K (~1777 °C). The experimental uncertainties given in Table II of (Bowen and Schairer, 1935) are ± 3 °C at the fayalite melting point rising to ±20 °C at the forsterite melting point. They also stated the accuracy of their solidus mea- surements (in terms of olivine composition) was up to 3–4% in the percentages of forsterite and fayalite. In contrast, their liq- uidus measurements have insignificant errors in the olivine com- position. Thus we believe our measured solidus is consistent with the pseudo-binary phase diagram.

The phase diagram in Fig. 1 (a) shows $Fo_{95}Fa_5$ olivine is in equi- librium with melt of composition $Fo_{79.5}Fa_{20.5}$ at the solidus (the horizontal dashed line and points). At the solidus, an infinites- imal amount of melt forms and if equilibrium between olivine crystals + melt is maintained during heating in the Knudsen cell, the fayalite content in the melt should move toward the upper left on Fig. 1 (a). For example, at 1850 °C olivine and melt in equilib- rium with each other (the small blue dots in Fig. 1 (a)) have com- positions of $Fo_{97}Fa_3$ and $Fo_{87}Fa_{13}$, and the system is ~80% olivine and 20% melt. At the liquidus (upper red dot at 1875 °C) the com- positions of olivine and melt have converged and the system is ~100% melt with an infinitesimal amount of solid and the same bulk composition $Fo_{95}Fa_5$.

However, our data taken above the solidus did not show this phenomenon. Instead it seems the crystals + melt did not equili- brate because significantly more Fe (than Mg) was vaporized from the two phase olivine + melt system in the Knudsen cell and al- most pure forsterite was left at the end. It is uncertain if the solid + melt equilibrated on the short time scale of our experiments because Bowen and Schairer (1935) stated it was impossible to prepare unzoned (ie., homogeneous) olivines for their solidus tem- perature measurements.

Incongruent melting of FeO-bearing olivine may account for our observations. Liquid Fe_2SiO_4 decomposes to produce Fe, Fe_2O_3, and SiO_2 (Stebbins and Carmichael, 1984)

$$0.9620\,Fe_2SiO_4(melt) + 0.0253\,Fe_2O_3(melt) + 0.0253\,Fe(liq) + 0.0280\,SiO_2(melt) \quad (34)$$

The Fe vapor pressure over Fe (liq) is larger than that over molten olivine, e.g., at 2050 K the values are $10^{-3.16}$ bar (liquid Fe) vs. $10^{-4.05}$ bar ($Fo_{95}Fa_5$ olivine). According to LeChatelier's Princi- ple, Fe loss due to vaporization causes more Fe_2SiO_4 (liq) to de- compose giving more liquid Fe, Fe_2O_3, and SiO_2. The Fe_2O_3 also vaporizes and is lost. Eventually none or almost none of the Fe is left and the remaining silica + forsterite react to form enstatite via

$$SiO_2(silica) + 2Mg_2SiO_4(forsterite) = 2MgSiO_3(protoenstatite) \quad (35)$$

If equilibrium is reached, this reaction proceeds until all silica is consumed; for our sample XRD shows the final molar ratio of forsterite to protoenstatite is 4 to 1, but a few percent of SiO_2, which is below the XRD detection limit, may still be present, as discussed earlier.

Table 5
(Fe/Mg) Atomic ratio in silicate vapor atmo- spheres of HRE.

Planet	Surface T (K) [a]	Fe/Mg [c]
Kepler 36b	1476	769
Kepler 93b	1569	360
KOI-2700b	1780	86
K2-22b	2135	15
CoRoT-7b	2425	5.1
early Earth	2500 [b]	4.0
55 Cnc e	2671	2.5
Kepler 10b	3007	1.1
Kepler 78b	3056	1.0
early Earth	3500 [b]	0.46

[a] Sub-stellar temperatures of exoplanets from Kite et al. (2016)

[b] Pahlevan et al. (2011) give 250 0–350 0 K for temperature of the Earth's silicate vapor atmosphere after the Moon-forming im- pact.

[c] From our modeling, see Section 4.7 for a discussion.

4.7. Implications for silicate atmospheres of hot rocky exoplanets (HRE)

Table 5 lists several hot rocky exoplanets (HRE), which have surface temperatures greater than 10 0 0 K at the sub-stellar point (assuming unit albedo, Kite et al., 2016). They are rocky based on their mass and radius (e.g., Fig. 4 of Dressing et al., 2015). The HRE are thought to have silicate vapor atmospheres (e.g., see Kite et al., 2016; Ito et al., 2015; Schaefer and Fegley, 2009) and our work gives constraints on the Fe/Mg atomic ratio in these atmospheres.

We discussed fractional vaporization of Fe and Mg from olivine in Section 4.2 . The equation describing this is plotted in Fig. 8 and is

[redacted] (36)

We used this equation to compute the (Fe/Mg) values listed in Table 5 and plotted in Fig. 11 . The surface temperatures at the sub- stellar point for each HRE were taken from Table 3 of Kite et al. (2016) . Pahlevan et al. (2011) give the low and high end of the tem- perature range (2500–3500 K) for the silicate vapor atmosphere on the Earth after the Moon-forming impact. Our results predict the $(Fe/Mg)_{gas}$ values will decrease with increasing surface tempera- ture as more Mg is vaporized from the magma oceans on these planets.

Prior theoretical studies predicted qualitatively similar behav- ior (e.g., Fig. 2 of Schaefer and Fegley, 2009 , Fig. 4 of Fegley and Schaefer, 2014 , Fig. 2 of Ito et al., 2015). For example, Fig. 2A of Ito et al. (2015) gives Fe/Mg ratios of 4.5, 2.7, and 1.3 at 20 0 0, 250 0, and 30 0 0 K, respectively. Fig. 4 of Fegley and Schaefer (2014) gives Fe/Mg ratios of 2.9, 1.1, and 0.6, respectively, at the same tempera- tures. Ito et al. (2015) used a regular solution model (MELTS) while Fegley and Schaefer (2014) and Schaefer and Fegley (2009) used an associated species model (MAGMA). Our results agree with both models (better with Ito et al., 2015), but are preferable because they are based on experimental vaporization data. In principle it should be possible to measure vaporization of minor and trace el- ements that substitute for Mg and Fe in olivine (e.g., Ni, Ca, Mn, Co) and predict their abundances in silicate vapor atmospheres but this is a topic for future study.

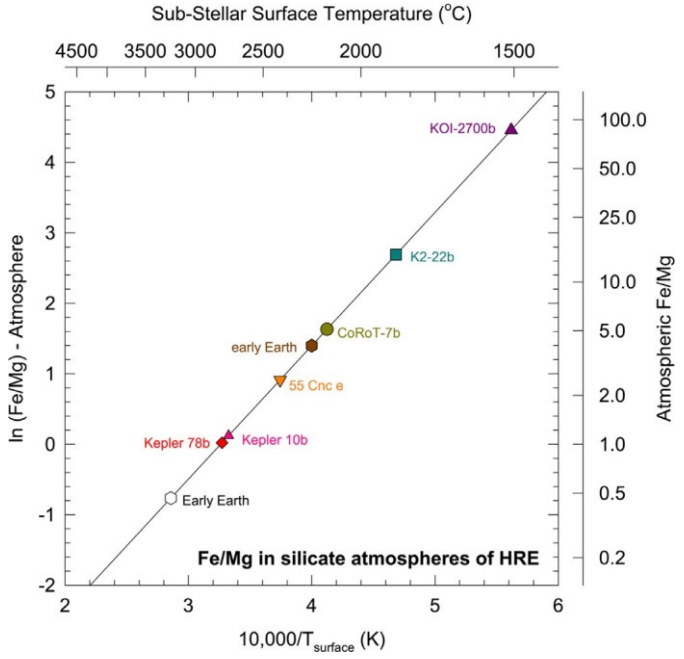

Fig. 11. Natural logarithm of Fe/Mg atomic ratio versus inverse temperature in sili- cate vapor atmospheres of HRE.

5. Summary and conclusions

The vaporization of olivine of composition Fo_{95} Fa_5 has been studied from 1750–2250 K. It was found that impurities in the mineral could be removed by heating in a vacuum at 1853 K for 10 h The vaporization behavior was studied with Knudsen Effu- sion Mass Spectrometry to obtain partial pressures as a function of inverse temperature. An iridium cell was fairly inert to olivine below the melting point; however there was some reaction above the melting point. The onset of melting was observed at ~2050 K, consistent with the literature. It was also observed that significant losses of the FeO component occurred at the melting point.

Thermodynamic data was taken on this composition below the melting point. The equilibrium constant for each component (MgO, Fe/FeO, and SiO_2) were compared to the equilibrium constant for the pure material. Thermodynamic activities and partial molar en- thalpies were derived for these components in olivine. By treat- ing the system as a Fo-Fa pseudo-binary, we derived the enthalpy and entropy of vaporization. Our data compared favorably to that of other investigators. Our data also showed that olivine fraction- ates with the FeO component vaporizing preferentially. By treating the system as a MgO–'FeO'–SiO_2 psuedo-ternary, we compare data to activities calculated from an assessed thermodynamic databases in the literature. We also used our data to derive total vapor pres- sures and concluded with some comments on possible silicate va- pors in the atmosphere of the hot, rocky exoplanets.

Acknowledgments

We are grateful to Dr. Olga Fabrichnaya (TU-Freiburg, Germany) for sharing her database and assistance with the calculations and R. Rogers (NASA Glenn) for assistance with X-ray diffraction.

This work was supported by NASA EPSCoR (Experimental Pro- gram to Stimulate Competitive Research). NNX13AE52A , "Understanding the Atmospheres of Hot Earths and the Impact on Solar System Formation" with NASA Glenn Research Center, Missouri State University and Washington University, St. Louis. GCCC is grateful to the ORAU/NASA Post-Doctoral Fellowship program for support. NSF Astronomy Program Grant AST-1412175 also sup- ported work by BF on this paper.

Supplementary materials

Supplementary material associated with this article can be found, in the online version, at doi:10.1016/j.icarus.2017.02.006 .

References

Andersson, J.O. , Helander, T. , Hoglund, L.H. , Shi, P.F. , Sundman, B. , 2002. THER- MO-CALC & DICTRA, computational tools for materials science. Calphad 26 (2), 273–312 .
Balducci, G. , De Maria, G. , Guido, M. , Piacente, V. , 1971. Dissociation Energy of FeO ₊. J. Chem. Phys. 55 (5), 2596–2598 .
Bale, C.W. , Chartrand, P. , Degterov, S.A. , Eriksson, G. , Hack, K. , Ben Mahfoud, R. , Melançon, J. , Pelton, A.D. , Petersen, S. , 2002. FactSage thermochemical software and databases. Calphad 26 (2), 189–228 .
Bowen, N. , 1913. The Melting Phenomena of the plagioclase feldspars. Am. J. Sci. 35, 577–599 .
Bowen, N. , Anderson, O. , 1914. The binary system MgO–SiO_2 . Am. J. Sci. 37, 487–500 .
Bowen, N. , Schairer, J.F. , 1932. The system, FeO–SiO_2 . Am. J. Sci. 24, 177–213 .
Bowen, N. , Schairer, J.F. , 1935. The system, magnesia-ferrous oxide-silica. Am. J. Sci. 29, 153 .
Bradley, J.P. , Humecki, H.J. , Germani, M.S. , 1992. Combined infrared and analytical electron microscope studies of interplanetary dust particles. Astrophys. J. 394, 643–651 .
Campins, H. , Ryan, E.V. , 1989. The indentification of crystalline olivine in cometary silicates. Astrophys. J. 341, 1059–1066 .
Cater, E.D. , 1979. The effusion method at age 69: current state of the art. In: Hastie, J.W. (Ed.), Characterization of High Temperature Vapors and Gasses Vol 1. NBS Special Publication 561/1, Washington, D.C .
Chekhovskoi, D.V. , Ivanisov, A.V. , Proskurnev, A.Y. , Press, C.R.C. , 1993. IVTANTHERMO database on thermodynamic properties of individual substances. NIST Special Database 5. CRC Press, Boca Raton .
Chestakov, D.A. , Parker, D.H. , Baklanov, A.V. , 2005. Iron monoxide photodissociation. J. Chem. Phys. 122 84302–84302 .
Copland, E.H. , Jacobson, N.S. , 2001. Thermodynamic activity measurements with Knudsen cell mass spectrometry. Electrochem. Soc. Interface (Summer) 28–31 .
Copland, E.H. , Jacobson, N.S. , 2010. Measuring Thermodynamic Properties of Metals and Alloys with Knudsen Effusion Mass Spectrometry .
Copland, E.H. , Auping, J.V. , Jacobson, N.S. , 2013. The process of developing a multi- -cell KEMS instrument. In: Proceedings of the Workshop on Knudsen Effusion Mass Spectrometry, 46, pp. 197–209 .
Cruikshank, D.P. , Hartmann, W.K. , 1984. The meteorite-asteroid connection: two olivine-rich asteroids. Science 223 (4633), 281–283 .
Dachs, E. , Geiger, C.A. , 2007. Entropies of mixing and Subsolidus phase relations of forsterite–fayalite (Mg_2SiO_4–Fe_2SiO_4) solid solution. Am. Mineral. 92, 699–702 .
Decterov, S.A. , Jung, I.H. , Pelton, A.D. , 2002. Thermodynamic modeling of the FeO–Fe_2O_3–MgO–SiO_2 system. J. Am. Ceram. Soc. 85 (12), 2903–2910 .
Dohmen, R. , Chakraborty, S. , Palme, H. , Rammansee, W. , 1998. Solid-solid reactions mediated by a gas phase: an experimental study of reaction progress and the role of surfaces in the system Olivine + Iron metal. Am. Mineral. 83, 970–984 .
Drowart, J. , Goldfinger, P. , 1967. Investigation of inorganic systems at high temper- ature by mass spectrometry. Angewandte Chemie 6 (7), 581–648 International Edition .
Dressing, C.D. , Charbonneau, D. , Dumusque, X. , Gettel, S. , Pepe, F. , Cameron, A.C. , Latham, D.W. , Molinari, E. , Udry, S. , Affer, L. , Bonomo, A.S. , Buchhave, L.A. , Cosentino, R. , Figueira, P. , Fiorenzano, A.F.M. , Harutyunyan, A. , Haywood, R.D. , Johnson, J.A. , -Morales, M.L. , Lovis, C. , Malavolta, L. , Mayor, M. , Micela, G. , Mo- talebi, F. , Nascimbeni, V. , Phillips, D.F. , Piotto, G. , Pollaco, D. , Queloz, D. , Rice, K. , Sasselov, D. , Ségransan, D. , Sozzetti, A. , Szentgyorgyi, A. , Watson, C. , 2015. The mass if Kepler-93b and the compositions of terrestrial planets. Astrophys. J. 800, 135 .
Drowart, J. , Chatillon, C. , Hastie, J. , Bonnell, D. , 2005. High-temperature mass spec- trometry: instrumental techniques, ionization cross-sections, pressure measure- ments, and thermodynamic data. Pure Appl. Chem. 77 (4), 683–737 .
Fabrichnaya, O. , 1998. The assessment of thermodynamic parameters for solid phases in the Fe-Mg-O and Fe-Mg-Si-O systems. Calphad 22 (1), 85–125 .
Fabrichnaya, O. , 20 0 0. Thermodynamic modelling of melting in the system FeO–MgO–SiO_2–O_2 at pressure of 1 bar. Calphad 24 (2), 113–131 .
Fegley Jr., B. , Cameron, A.G.W. , 1987. A vaporization model for iron/silicate fraction- ation in the Mercury protoplanet. Earth Planet. Sci. Lett. 82, 207–222 .
Chapter 6.3 Fegley Jr., B. , Schaefer, L.K. , 2014. Chemistry of the Earth's earliest atmo- sphere. In: Farquhar, J., Canfield, D., Kasting, J. (Eds.), The Atmosphere - History. In: Treatise on Geochemistry, vol 13. Elsevier Science, pp. 71–90 .
Field, F.H. , Franklin, J.L. , 2013. Electron Impact Phenomena: And the Properties of Gaseous Ions. Academic Press .
Hildenbrand, D.L. , 1975. Thermochemistry of molecular FeO, FeO ₊ and FeO. Chem. Phys. Lett. 34 (2), 352–354 .
Hirth, J.P. , 1967. Evaporation and Sublimation Mechanisms. In: Margrave, J.L. (Ed.), The Characterization of High Temperature Vapors, Chapter 15. John Wiley & Sons, Inc., New York, NY, pp. 453–472 .
Hoefen, T.M. , Clark, R.N. , Bandfield, J.L. , Smith, M.D. , Pearl, J.C. , Christensen, P.R. , 2003. Discovery of olivine in the Nili Fossae region of Mars. Science 302, 627–630 .
Hultgren, R. , Desai, P.D. , Hawkins, D.T. , Gleiser, M. , Kelley, K.K. , 1973. Selected Values of the Thermodynamic Properties of the Elements DTIC Document .

Ito, Y. , Ikoma, M. , Kawahara, H. , Nagahara, H. , Kawashima, Y. , Nakamoto, T. , 2015. Theoretical emission spectra of atmospheres of hot rocky super-Earths. Astro- phys. J. 801, 144 .
Kato, E. , 1993. Thermodynamic studies of metallurgical systems by mass spectrom- etry. J. Mass Spectrom. Soc. Jpn. 41 (6), 297–316 .
Keil, K. , Bunch, T.E. , Prinz, M. , 1970. Mineralogy and composition of Apollo 11 Lu- nar samples. In: Proceedings of the Apollo 11 Lunar Science Conference, 1, pp. 561–598 .
Kitayama, K. , Katsura, T. , 1968. Activity measurements in orthosilicate and metasil- icate solid solutions. I. Mg_2SiO_4-Fe_2SiO_4 and $MgSiO_3$-$FeSiO_3$ at 1204 °C. Bull. Chem. Soc. Jpn. 41 (5), 1146–1151 .
Kite, E.S. , Fegley Jr., B. , Schaefer, L. , Gaidos, E. , 2016. Atmosphere-interior exchange on hot, rocky exoplanets. Astrophys. J. 828, 80 .
Kojima, Y. , Inouye, M. , Sano, K. , 1969. The activity of the iron oxide in FeO–MgO–SiO_2 slags at 1600 °C. Arch Eisenhuttenwesen 40 (1), 37–40 .
Larimer, J.W. , 1968. "Experimental studies on the system Fe–MgO–SiO_2–O_2 and their bearing on the petrology of chondritic meteorites. Geochim. Cosmochim. Acta 32, 1187–1207 .
Lee, K.N. , Worrell, W.L. , 1989. The oxidation of iridium-aluminum and iridi- um-hafnium intermetallics at temperatures above 1550 °C. Oxid. Met. 32 (5-6), 357–369 .
Levin, R.D., Lias, S.G., 1982. Ionization Potential and Appearance Potential Mea- surements, 1971–1981. National Bureau of Standards, United States from http: //purl.access.gpo.gov/GPO/LPS113176 .
Liebau, F. , 2012. Structural Chemistry of Silicates: Structure, Bonding, and Classifica- tion. Springer Science & Business Media .
Lodders, K. , 2003. Solar system abundances and condensation temperatures of the elements. Astrophys. J. 591, 1220–1247 .
Lodders, K. , Palme, H. , Gail, H.P. , 2009. Abundances of the elements in the solar sys- tem. Chapter 4.4 in Solar System vol 4B. In: Trumper, J.E. (Ed.), Landolt–Born- stein Tables. Springer Verlag, Berlin, pp. 712–770 .
Mann, J.B. , 1967. Ionization cross sections of elements calculated from mean-square radii of atomic orbitals. J. Chem. Phys. 46 (5), 1646–1651 .
Muan, A. , 1967. Determination of thermodynamic properties of silicates from loca- tions of conjugation lines in ternary systems. Am. Mineral. 52, 797–804 .
Murad, E. , 1980. Thermochemical properties of gaseous FeO and FeOH. J. Chem. Phys. 73, 1381–1385 .
Mysen, B.O , Kushiro, I. , 1988. Condensation, evaporation, melting, and crystallization in the primitive solar nebula: experimental data in the system MgO–SiO_2–H_2O to 1.0×10^{-9} bars and 1870 °C with variable oxygen fugacity. Am. Mineral. 73 (1), 1–19 .
Nafziger, R.H. , Muan, A. , 1967. Equilibrium phase compositions and thermodynamic properties of olivines and pyroxenes in system MgO–FeO–SiO_2 . Am. Mineral. 52 (9-10), 1364–1385 .
Nagahara, H. , Kushiro, I. , Mysen, B.O. , Meri, H. , 1988. Experimental vaporization and condensation of olivine solid solution. Nature 331 (6156), 516–518 .
Nagahara, H. , Kushiro, I. , 1989. Vaporization experiments in the system plagio- clase–hydrogen. In: Proc NIPR Symposium Antarctic Meteorites, 2, pp. 235–251 .
Nagahara, H. , 1990. Vaporization experiments in the system plagioclase–hydro- gen: 2. Composition of the gas. In: Lunar Planetary Science Conference, 21, pp. 837–838 .
Nagahara, H. , Kushiro, I. , Mysen, B.O. , 1993. Vaporization and condensation of chon- dritic materials–experimental studies. In: Oya, H. (Ed.), Primitive Solar Nebula and Origin of Planets. Terra Scientific Publishing, Tokyo, pp. 427–446 .
Nagahara, H. , Kushiro, I. , Mysen, B.O. , 1994. Evaporation of olivine: low pressure phase relations of the olivine system and its implication for the origin of chondritic components in the solar Nebula. Geochim. Cosmochim. Acta 58 (8), 1951–1963 .
Navrotsky, A. , 1978. Thermodynamics of element partitioning: (1) systematics of thansition metals in crystalline and molten silicates and (2) defect chemistry and "the henry's law problem. Geochim. Cosmochim. Acta 42, 887–902 .
Nguyen, A.N. , Zinner, E. , 2004. Discovery of ancient silicate stardust in a meteorite. Science 303, 1496–1499 .
Ozawa, H. , Nagahara, H. , 20 0 0. Kinetics of diffusion-controlled evaporation of Fe-Mg olivine: experimental study and implication for stability of fe-rich olivine in the solar Nebula. Geochim. Cosmochim. Acta 64 (5), 939–955 .
Pahlevan, K. , Stevenson, D.J. , Eiler, J.M. , 2011. Chemical fractionation in the silicate vapor atmosphere of the earth. Earth Planet. Sci. Lett. 301, 433–443 .
Palme, H. , O'Neill, H.StC. , 2014. Cosmochemical estimates of mantle composition. Treatise on Geochemistry, 2nd ed. Chapter 3.1. Elsevier, Amsterdam, Nether- lands .
Pauling, L. , 1960. The Nature of the Chemical Bond. Cornell university press Ithaca, NY .
Piacente, V. , Matousek, J. , Spoliti, M. , Dipaolo, V. , 1975. Mass-spectrometric investi- gation of olivine vaporization process. Silikaty 19 (4), 289–300 .
Plante, E.R. , Hastie, J.W. , Kowalska, M. , 1992. Activity of FeO in the FeO–MgO–SiO_2 system determined by high-temperature mass-spectrometry. ISIJ Int. 32 (12), 1276–1279 .
Preston-Thomas, H. , 1990. International temperature scale of 1990 (ITS-90). Metrolo- gia 27, 3–10 .
Sakawa, M. , Whiteway, S. , Masson, C. , 1976. Activities of FeO in the ternary system SiO_2–MgO–FeO and constitution of SiO_2 . Tetsu to Hagane 62, 176–181 .
Saxena, S. , Chatterjee, N. , Fei, Y. , Shen, G. , 1993. Thermodynamic Data on Oxides and Silicates: An Assessed Data Set Based on Thermochemistry and High Pressure Phase Equilibrium. Springer-Verlag, Berlin, p. 428 .
Schaefer, L. , Fegley Jr., B. , 2009. Chemistry of silicate atmospheres of evaporating super-Earths. Astrophys. J. 703, L113–L117 .
Smoes, S. , Drowart, J. , 1984. Determination of the dissociation energies of gaseous iron monoxide and manganese monoxide by the mass spectrometric Knudsen cell method. In: Modern High Temperature Science. Humana Press, pp. 31–52 .
Stebbins, J.F. , Carmichael, I.S.E. , 1984. The heat of fusion of fayalite. Am. Mineral. 69 (3-4), 292–297 .
Stolyarova, V.L. , Semenov, G.A. , Beynon, J.H. , 1994. Mass Spectrometric Study of the Vaporization of Oxide Systems. Wiley, Chichester, New York .
Swierczynski, D. , Courson, C. , Bedel, L. , Kiennemann, A. , Guille, J. , 2006. Charac- terization of Ni-Fe/MgO/Olivine catalyst for fluidized bed steam gasification of biomass. Chem. Mater. 18 (17), 4025–4032 .
von Seckendorff, V. , O'Neill, H.S.C. , 1993. An experimental study of Fe-Mg partition- ing between olivine and orthopyroxene at 1173, 1273 and 1423 K and 1.6 GPa.. Contrib. Mineral. Petrol. 113 (2), 196–207 .
Wiser, N.M. , Wood, B.J. , 1991. Experimental Determination of Activities in Fe-Mg Olivine at 1400 K. Contrib. Mineral. Petrol. 108 (1), 146–153 .
Woolf, N.J. , Ney, E.P. , 1969. Circumstellar infrared emission from cool stars. Astro- phys. J. 55, L181–L184 .
Wriedt, H.A. , 1991. The Fe-O (Iron-Oxygen) system. J. Phase Equilib. 12 (2), 170–200 .
Wu, P. , Eriksson, G. , Pelton, A.D. , Blander, M. , 1993. prediction of the thermo- dynamic properties and phase diagrams of silicate systems-evaluation of the FeO–MgO–SiO_2 system. ISIJ Int. 33 (1), 26–35 .